Supporting information

The oxidation of platinum under wet conditions observed by electrochemical X-ray photoelectron spectroscopy

Rik Mom[1]*, Lorenz Frevel[1], Juan-Jesús Velasco-Vélez[1], Milivoj Plodinec[1,2], Axel Knop-Gericke[1], Robert Schlögl[1]

1. Fritz-Haber-Institut der Max-Plack-Gesellschaft, Faradayweg 4-6, 14195 Berlin, Germany
2. Rudjer Boskovic Institute, Bijenicka 54, 10000 Zagreb, Croatia

*mom@fhi-berling.mpg.de

S1 Sample preparation

The Nafion® 117 membranes were cleaned in 3 w% H_2O_2 in water at 80 ºC for 2 hours, followed by activation in 0.5 M H_2SO_4 at the same temperature, also for 2 hours. The membranes were subsequently washed in ultrapure water and stored dry.

Platinum (Electronen-Optik-Service GmbH target) was sputter-deposited onto the membranes using a Cressington 208 HR sputtercoater in argon plasma. For the TEM measurements, Quantifoil Au 200 R1.2/1.3 grids (coated with holey carbon) were covered with a thin Nafion film (see Figure S1a) by dip coating in a resin solution (5 wt% Nafion in lower alcohols, Sigma Aldrich), which was diluted 10x in ethanol. EDX mapping of sulfur and fluorine showed that this procedure yields a uniform Nafion film. Unfortunately, no resin solution was available for the FAD membrane. To assess the sensitivity of the particle size distribution to the deposition substrate, we compared Pt sputtered on Nafion with Pt sputtered on the bare carbon film (Figure S1b,c). The latter is likely closer to the situation for FAD, which is a (functionalized) polyarylether. Figure S1 shows only minor differences between Pt/Nafion and Pt/carbon, with slightly smaller particles in the case of Nafion.

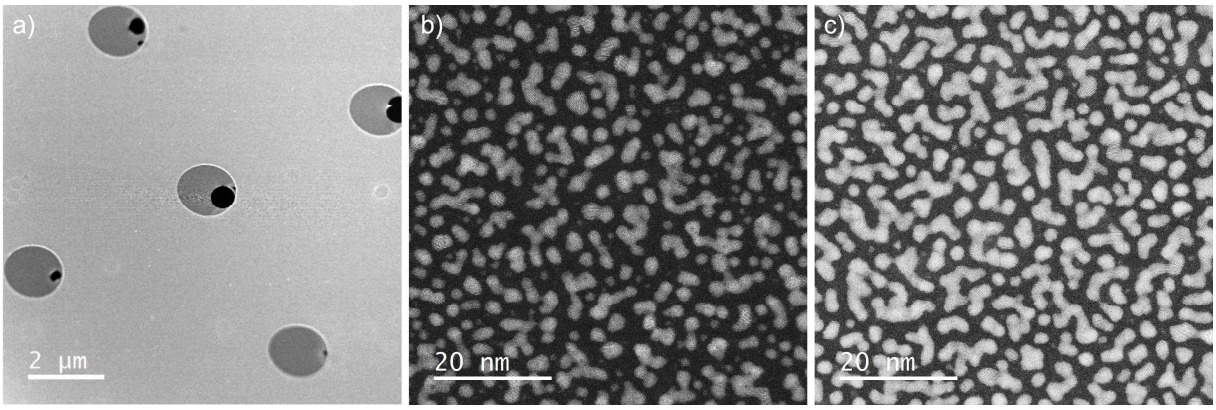

Figure S1: Electron microscopy study of the sputtered particles. a) SEM image of Nafion film covering the holey carbon film of a Quantifoil TEM grid. b) TEM image of Pt on Nafion (film deposited Quantifoil). c) TEM image of Pt on carbon (Quantifoil)

To investigate the cleanliness of the deposition process, Figure S2 shows a comparison of the dark field and bright field TEM images of the same particle. The dark field image is predominantly sensitive to heavy elements (e.g. Pt), whereas the bright field image allows the observation of light elements (e.g. C contamination). The overlay of the two images (Figure S2c) shows excellent matching, which confirms the absence of a contaminant layer. We should point out, however, that a single layer of small adsobates following air exposure will have likely formed, and would be beyond the detection sensitivity of the analysis.

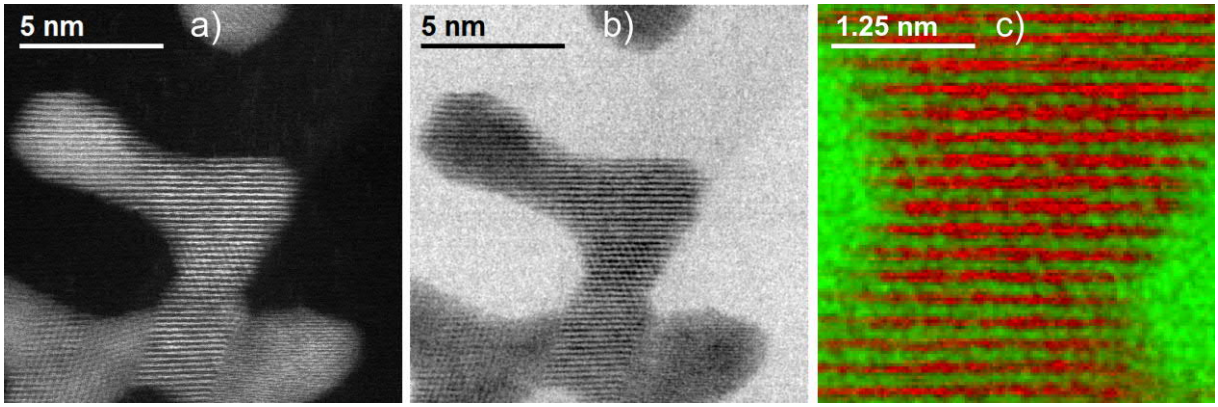

Figure S2: High-resolution TEM analysis of the surface cleanliness of the sputtered Pt particles. For the TEM analysis, the particles were sputtered on Quantifoil Au 200 R1.2/1.3 coated with holey carbon. a) Dark field image, as also shown in Figure 1c in the main text. b) Corresponding bright field image. c) Overlay of dark field (red) and bright field (image).

Following the deposition, the FAD55 membranes were soaked in 0.5 M Na_2SO_4 at room temperature for at least 3 days. The Nafion® samples were kept dry.

Graphene on copper (Graphenea SA) was etched in a 40 g/L $(NH_4)_2S_2O_8$ aqueous solution to remove the copper substrate, leaving a floating graphene sheet on the water surface. After dilution of the solution, the membranes were introduced into the water beneath the graphene sheets. Subsequently, the water level was lowered to transfer the graphene onto the membranes. Following the transfer, the samples were dried in air at room temperature to ensure adhesion of the graphene layer. To prevent the formation of microtears in the FAD55 membranes due to repetitive swelling and drying, the FAD55 membranes were reintroduced to the 0.5 M Na_2SO_4 solution after approximately 15 minutes of drying (only the surface of the membrane is completely dry under these conditions). Prior to use, the membranes were washed in ultrapure water.

Figure S3 shows XPS surveys of graphene-covered Pt on Nafion® (S3a) and on FAD55 (S3b). As expected for the thin, open layers studied here, the Pt layer does not obscure the underlying membrane from XPS observation. For Nafion®, a fluoro-ether with sulfonate functionalization, we observe this in the form of F, O and S peaks. Similarly, N, C, and O can be related to FAD55 in Figure S3b. In addition, FAD55 contains Br. As shown in the main text however, these species only become apparent at high potential (see also Figure 2 in the main text). The only contamination visible in the spectra is a minute Cu LMM Auger peak. This can be attributed to remnants of Cu left after the graphene preparation procedure. We should point out that these remnants do not appear to be the result of insufficient etching. In fact, the Cu substrate is not visible anymore after only 1 hour of etching, whereas the total

etching time was 12 hours. Hence, it seems likely that the Cu remnants are encapsulated in defective parts of the graphene.

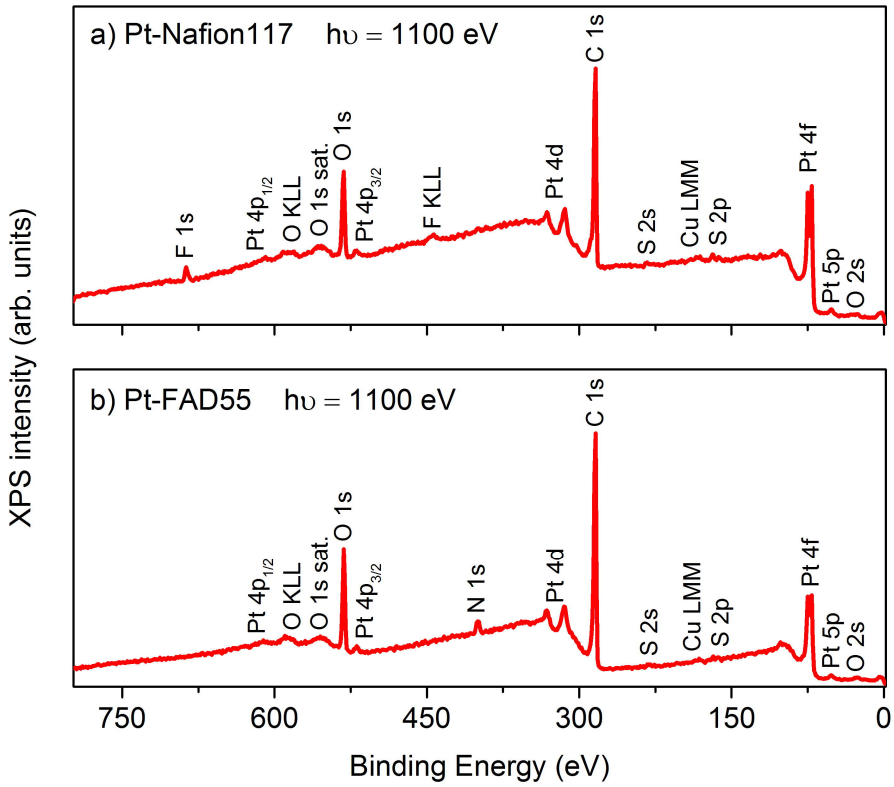

Figure S3: XPS survey spectra of a) 4 nm graphene-covered Pt on Nafion® 117 (corresponding to Figure 5b in the main text) and b) 1 nm graphene-covered Pt on Fumasep® FAD55 (corresponding to Figure 4 in the main text). Both spectra were recorded in the electrochemical cell at OCP. In both cases, the electrolyte was 0.1 M H_2SO_4.

The graphene layer attenuates the Pt 4f signal due to scattering of the photoelectrons. We established that 300 eV electron kinetic energy is the lower bound for our measurements. Most experiments were conducted with a kinetic energy of roughly 500 eV. Under these conditions the transmission through the graphene is about 40%, estimated using the data at OCP shown in Figure 2 b and c in the main text.

Along with the spectroscopic measurements, we performed an electrochemical characterization of the samples in situ at the beam line. For a proper judgement of the electrochemical data, we should point out that a large fraction of the sample was in contact with the glassy carbon top plate, which contains a hole for spectroscopy (see Figure S4a). Hence, the electrochemical data reflect not only the bare or graphene covered part of the sample, but also the part where the Pt catalyst is sandwiched between the proton exchange membrane and the glassy carbon top plate.

Impedance measurements for both the Nafion® and FAD55 supported samples indicated a contact/solution resistance of 40-50 Ω at OCP. Figures S4b-d show cyclic voltammetry data recorded at the beamline. The Nafion® sample in Figure S4b shows the usual Pt features: surface oxidation onset (OH/O adsorption) at roughly 0.8 V, the oxygen evolution onset at about 1.55 V, the oxide reduction in the cathodic scan at 0.65 V, hydrogen adsorption features between 0.2 V and 0 V and the hydrogen evolution below 0 V. In addition, a large peak is observed at 0.05 V. We attribute this to the oxidation of H_2 gas, which may require some time to diffuse away from the glassy carbon-Pt-membrane sandwich. The graphene-covered Pt/FAD55 sample in Figure S4c shows the same features, although the CV is also modified by the electrochemical behavior of the FAD55 membrane itself (Figure S4d).

XPS was used as a probe for the conductivity in the working electrode. For a grounded electrode, the Pt^0 peak should remain at the same position independent of the applied potential. If electrical contact is lost, the Pt^0 peak will shift to lower binding energy at positive potentials, which easily distinguishes this behavior from Pt oxidation. The same holds for the position of the valence band edge. By checking these two factors, it was established that the electrical contact of all the samples shown in this work was adequate.

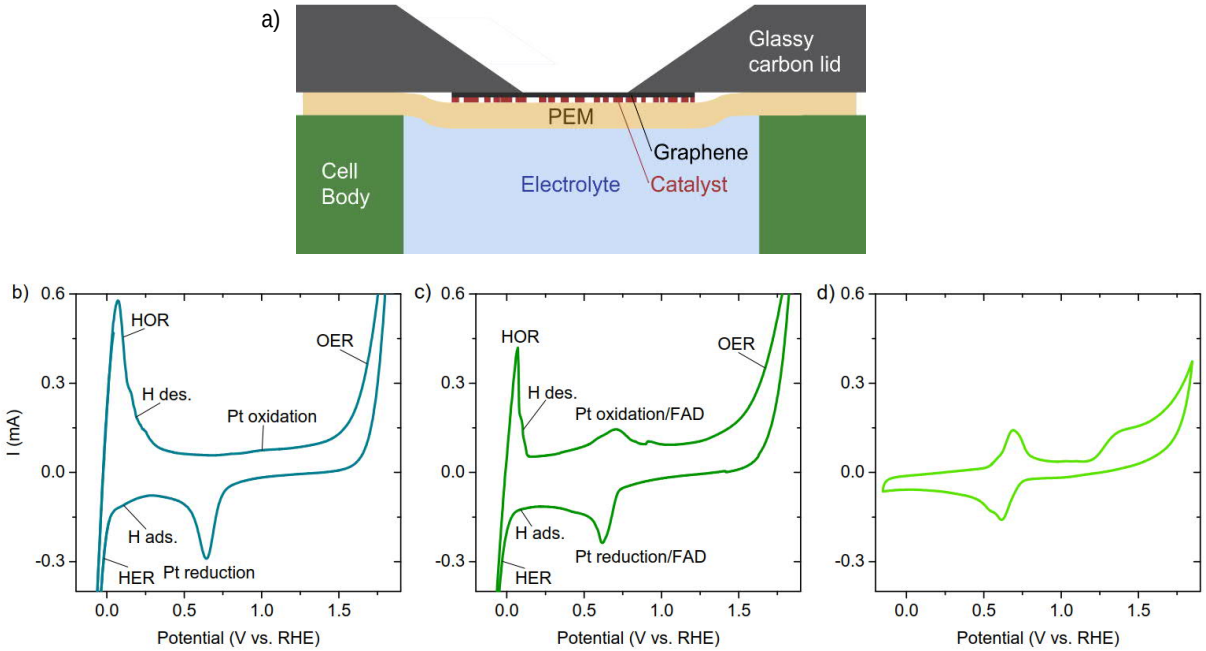

Figure S4: Cyclic voltammetry recorded at the beamline at 20 mV/s with 0.1 M H_2SO_4 electrolyte. a) Schematic representation of the working electrode assembly. Cyclic voltammograms are shown for b) 16 nm Pt on Nafion®. c) 16 nm graphene-covered Pt on FAD55. d) Bare FAD55. As is evident from a) the glassy carbon contact plate also contributes to the electrochemical current. Abbreviations for the indicated processes: hydrogen oxidation reaction (HOR), hydrogen reduction reaction (HER), hydrogen adsorption (H ads.), hydrogen desorption (H des.), oxygen evolution reaction (OER), electrochemical response of the FAD membrane (FAD).

To test the performance of the system under reaction conditions, we used mass spectrometry to detect O_2 generated at on the Pt catalyst at 1.85 V. As shown in Figure S5, our catalyst is clearly able to provide a steady-state conversion, despite the poor quality of platinum as a catalyst for the oxygen evolution reaction. In agreement with this, impedance measurements showed that the resistance between the reference electrode and working electrode was a modest 50 Ohm, implying good mass transport through the membrane.

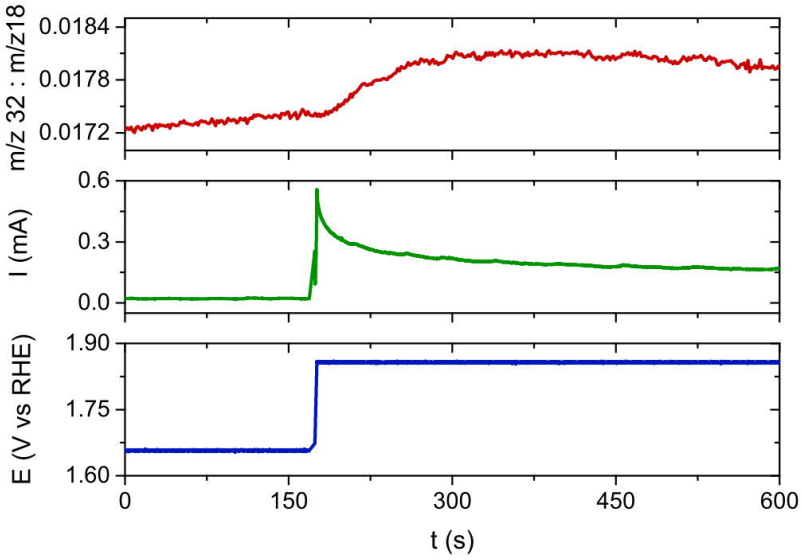

Figure S5: Oxygen evolution reaction on 16 nm graphene-covered Pt on FAD55.

S2 Analysis procedure

Analysis of the XPS spectra was performed using the CasaXPS 2.3.18 software package. A Shirley background subtraction was used in all cases. The asymmetric Lorentzian LF lineshape was used for fitting of the Pt 4f spectra. While the Doniach-Sunjic lineshape is more physically rigorous, the dampened tail of the LF curve ensures a more unambiguous fit within the limited spectral window that we afforded ourselves in order to limit beam damage. Fitting was performed using 4 doublets: Pt^0, $Pt^{\delta+}$, Pt^{2+} and Pt^{4+}, parameterized as shown in Tables S1-S4. The first two parameters in the LF line shape define the peak asymmetry (equal means symmetric, large difference results in an asymmetric lineshape), the third parameter refers to the width of the Gaussian with which the Lorenzian curve is convoluted and the forth parameter defines the dampening of the curve away from the peak center. The more symmetric lineshape used for the Pt^{4+} contribution was chosen not only based on the observed peak shape at high potential, but also based on the physical nature of poorly conducting materials such as PtO_2, which have less peak asymmetry due to their limited electron-hole pair excitations.

Table S1: Fitting parameters for Pt 4f spectral decomposition for 480 eV and 600 eV excitation energy

	Pt^0	$Pt^{\delta+}$	Pt^{2+}	Pt^{4+}
Lineshape	LF(0.63, 2, 20, 50)	LF(0.63, 2, 20, 50)	LF(0.63, 2, 20, 50)	LF(1.8,2,20,0)
Peak position	70.9 to 71.1 eV	71.2 to 72.0 eV	72.0 to 72.7 eV	Determined at highest potential of the dataset
FWHM	Free	Same as Pt^0	Same as Pt^0	Determined at highest potential of the dataset

Table S2: Fitting parameters for Pt 4f depth profiling at 1.85 V_{RHE}, excitation energy 380 eV

	Pt^0	$Pt^{\delta+}$	Pt^{2+}	Pt^{4+}
Lineshape	LF(0.63, 2, 20, 50)	LF(0.63, 2, 20, 50)	LF(0.63, 2, 20, 50)	LF(1.8,2,20,0)
Peak position	70.9 to 71.0 eV	71.95 to 72.0 eV	72.3 to 72.7 eV	73.5 , 73.4
FWHM	1.065 eV	1.065 eV	1.065 eV	1.25 eV

Table S3: Fitting parameters for Pt 4f depth profiling at 1.85 V_{RHE}, excitation energy 780 eV

	Pt^0	$Pt^{\delta+}$	Pt^{2+}	Pt^{4+}
Lineshape	LF(0.9,2,20,50)	LF(0.9,2,20,50)	LF(0.9,2,20,50)	LF(1.8,2,20,0)
Peak position	70.9 to 71.0 eV	71.95 to 72.0 eV	72.3 to 72.7 eV	73.5 , 73.4
FWHM	1.2 eV	1.2 eV	1.2 eV	1.53 eV

Table S4: Fitting parameters for Pt 4f depth profiling at 1.85 V_{RHE}, excitation energy 1280 eV

	Pt^0	$Pt^{\delta+}$	Pt^{2+}	Pt^{4+}
Lineshape	LF(0.9,2,20,50)	LF(0.9,2,20,50)	LF(0.9,2,20,50)	LF(1.8,2,20,0)
Peak position	70.9 to 71.0 eV	71.95 to 72.0 eV	72.3 to 72.7 eV	73.5 , 73.4
FWHM	1.35 eV	1.35 eV	1.35 eV	1.65 eV

The ranges for the peak positions were set according to literature data (see literature compilation in the supporting information of Saveleva et al.[1]). The binding energy of Pt^0 was allowed a +/- 0.1 eV variation to account for inaccuracies in setting the beam energy (valence band alignment was regularly performed during the beam time, but was inhibitively inaccurate for the low-coverage samples). For the depth profiling analysis the line shape, peak position and FWHM for Pt^0 and $Pt^{\delta+}$ were determined at open circuit potential, where no oxide was present. The parameters for the Pt^{4+} peak were determined by free fitting of the 4 nm thick sample at 1.85 V_{RHE}. In the other datasets, the line shape, peak position and FWHM of Pt^{4+} peak constrained to values from the 4 nm case.

For the O K-edge spectra, the energy scale was calibrated using the sharp peak at 537.2 eV in the TEY signal, belonging to the Rydberg state in gas-phase water[2]. The intensities were corrected for the synchrotron ring current and beam line transmission function. After applying an offset to set the pre-edge region to zero, the spectra were normalized to 1 at 552 eV.

S3 Beam damage effects and prevention measures

The intense X-rays employed in synchrotron measurements can be damaging to materials, in particular oxides and polymers. To investigate the effect of the beam on our samples we compare spectra at the start of beam exposure and after some minutes. As shown in Figure S6a, beam damage effects can be rather severe for the Nafion® samples. The PtO_2 is quite strongly reduced after roughly 4 minutes in the beam. In contrast, hardly any PtO_2 reduction is observed for the FAD55 sample (Figure S6b). This rather unexpected difference in behavior underlines the complexity of beam damage phenomena, and the need to study them for individual material combinations.

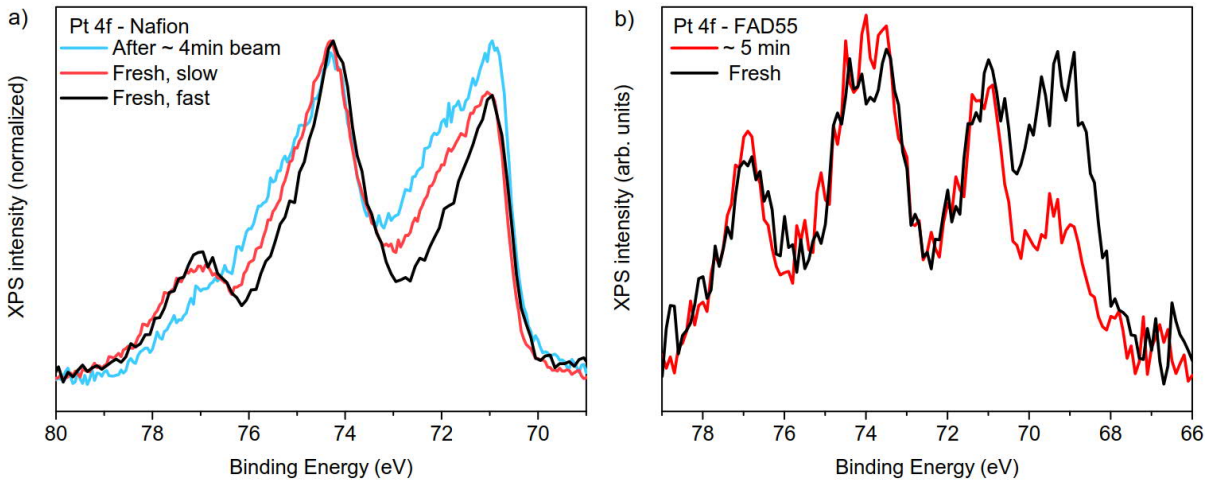

Figure S6: Beam exposure effects on the a) 4 nm graphene-covered Pt on Nafion® at 1.85 V with 580 eV excitation energy, and b) 16 nm graphene-covered Pt on FAD55 at 1.85 V with 380 eV excitation energy. In a), slow indicates a recording time of about 1 minute, as opposed to fast recording in 30 seconds.

While Pt oxides are stable on FAD55, the drop in the Br peak (Figure S6b) clearly indicates that the membrane polymer is damaged. To test if this affects the local proton conductivity, we compared the degree of electrochemical PtO_x formation on a beam exposed and a fresh spot for both Nafion® and FAD55. For the Nafion® case, we observed that the reactivity is suppressed on the exposed spot, whereas little to no effect was observed for FAD55. Hence, we conclude that while both Nafion® and FAD55 suffer beam damage, only Nafion® loses its proton conductivity as a result of this. Note that Nafion® and FAD55 have similar proton conductivities in their pristine form (as determined by their manufacturers).

The above results make clear that long beam exposure to our samples is undesirable, particularly for the Nafion® samples. For this reason, spectra were either recorded in a single (fast) scan and/or with low beam intensity (Figure 6a in the main text). Furthermore, each spectrum shown in the main text was recorded on a fresh spot on the surface. Due to the excellent homogeneity of our samples, and our relatively large beam spot size (0.2 mm x 0.1 mm), we do not expect significant variation the behavior of the sample on different spots on the surface. The smooth trends in the Pt 4f and O K-edge spectra confirm this.

S4 Wetting of the Pt nanoparticles

As discussed in the main text, the most important feature that can be used to investigate the wetting of the Pt nanoparticles is the peak at 535 eV in the O K-edge spectra. To determine the contribution of graphene oxide to this peak, Figure S7 shows O K-edge spectra of graphene deposited on a polycrystalline Au/Si substrate. To reduce the noise in the PEY spectrum, an average was taken of 5 spectra recorded at different locations on the surface. The ratio between the 535 eV peak and the peak at 532 eV that accompanies it is close to one. Given the small 532 eV contribution in Figure 2a in the main text, graphene oxide can only have a minor contribution to the observed 535 eV peak. Hence, it predominantly originates from water. It should be noted that the sulfate concentration on the surface was clearly higher for the graphene covered sample, as determined from the S 2p peak area. However, the O K-edge spectrum of sulfate does not show any peaks in the window between 530 eV and 537 eV[3,4].

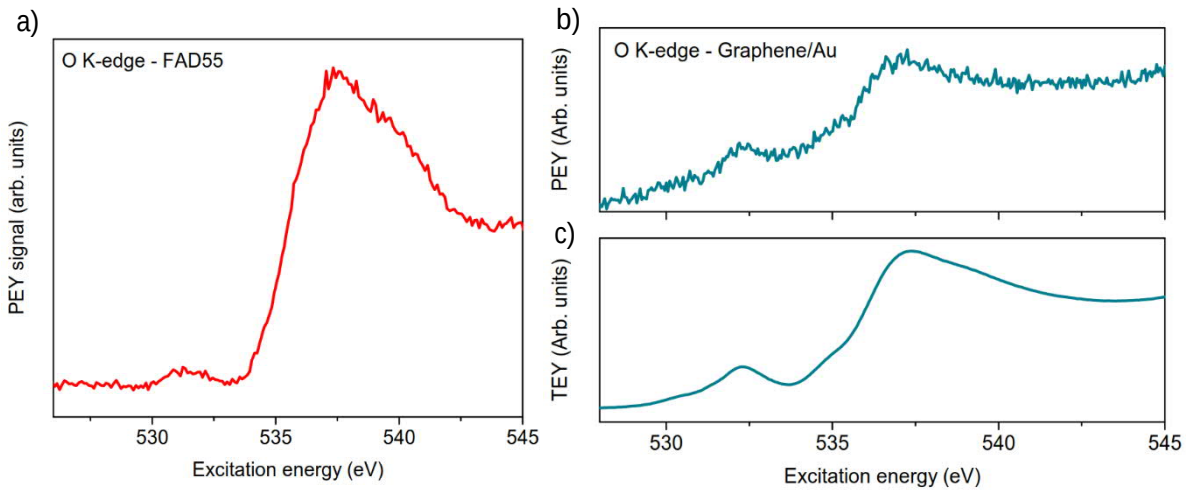

Figure S7: O K-edge spectrum of FAD55 and graphene. a) O K-edge spectrum of FAD55 with 0.1 M H_2SO_4 electrolyte. b) O K-edge spectrum of graphene deposited on a polycrystalline Au/Si substrate, recorded in PEY mode. c) Same, but recorded in TEY mode.

Some additional information on the wetting of the Pt particles can be obtained from the O 1s spectra. However, the large variety of species (H_2O_{ad}, $H_2O_{multilayer}$, membrane hydrocarbons, graphene oxide and SO_4^{2-}) in a limited spectral window (530-535 eV) make assignments extremely difficult. In addition, attenuation of the substrate, sulfate and water peaks due to the graphene layer hamper the comparison of intensities. Nonetheless, Figure S8 shows that a broadening of the O 1s spectrum occurs as a result of the graphene cover. The reference spectrum of graphene on Au shows that the broadening at higher binding energy is not related to graphene. The O 1s peak of sulfate is found between 532.1 and 532.5 eV[5], also disqualifying it as an explanation. With a binding energy of 533 eV, multilayer water would explain the broadening at higher binding energy, providing another indication for the high degree of wetting on the Pt samples.

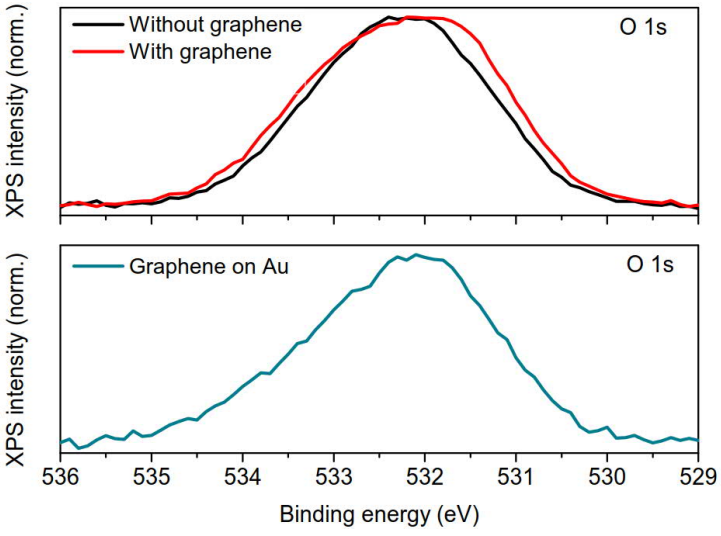

Figure S8: O 1s spectra of 16 nm Pt on FAD55 with and without graphene cover (a) and of graphene on a polycrystalline Au/Si substrate (b).

S5 Pt depth profiling with and without graphene

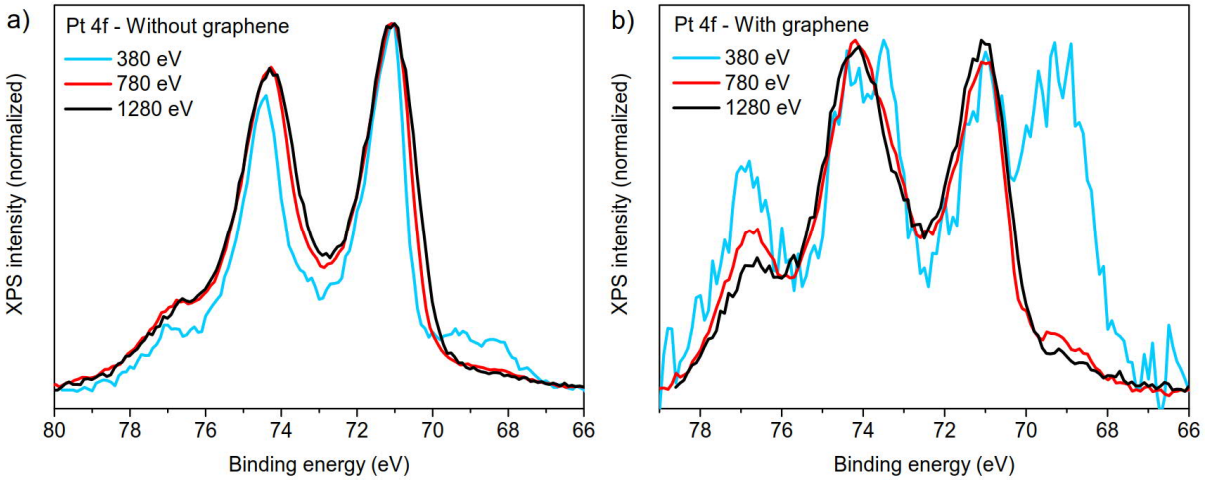

Figure S9: Depth profile of 16 nm Pt on FAD55 without (a) and with (b) graphene cover, recorded at 1.85 V_{RHE} following the stepwise oxidation procedure depicted in Figure 2 in the main text.

To establish the location of the electrochemically created oxide on the 16 nm thick Pt layers, we recorded Pt 4f spectra at several excitation energies. In the probed energy range, 380 eV to 1280 eV, the electron attenuation length in platinum changes from 0.54 nm to 1.16 nm[6]. Hence, the decrease in the Pt^{4+} peak at higher excitation energy seen in Figure S9b indicates that the XPS spectra probe an oxide at the outer surface of the catalyst layer (the graphene side). This is clearly not the case for the uncovered sample (Figure S9a), where the Pt^{4+} peak rises with excitation energy. Although some of the rise is related to the decreased spectral resolution at higher excitation energy, this suggests that the oxide is located at the buried Pt-FAD interface.

S6 XPS analysis of the electrolyte species in Nafion

Similar to the case of FAD, the binding energy of species belonging to the Nafion® membrane display shifts resulting from changes in the local electrostatic potential. As shown in Figure S10, the extent of the shifts varies. The C1s peak around 291 eV, which belongs to the fluorinated carbon in Nafion®, shifts 1.05 eV, roughly the expected 1.1 eV. In contrast, the peak at 284 eV, originating from the graphene cover layer, does not show any shift as it is part of the working electrode (which, again, was grounded via the electron analyzer). The O 1s peak shows a mixed response with a shift of 0.43 eV, indicating that the peak contains contributions from both species adsorbed on the working electrode and free electrolyte. For the fluorine signal, the importance of probing depth becomes evident. For the F1s peak, which is very surface sensitive due to the low kinetic energy of the emitted electrons (about 412 eV), a shift of 0.73 eV is observed. In contrast, the F KLL signal is shifted by 1.14 eV. Hence, it appears that the species probed by the F1s peak are predominantly located within the decay length of the electrostatic potential.

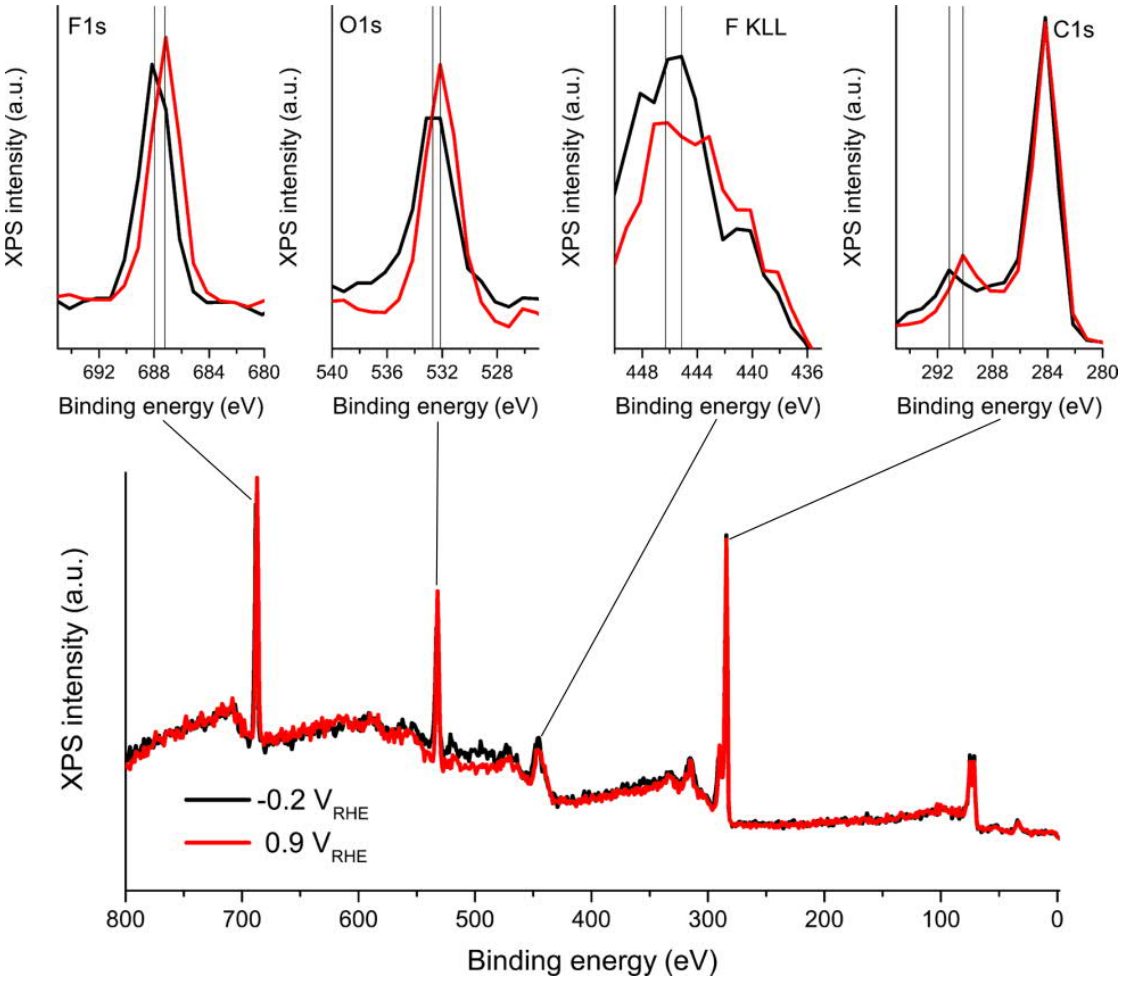

Figure S10: Influence of the local electrostatic potential on Nafion® XPS peak positions. Survey spectra of 1 nm graphene-covered Pt on Nafion®, with an excitation energy of 1100 eV and 0.1 M H_2SO_4 electrolyte.

S7 Potential-induced redistribution of the membrane in the catalyst layer

The shoulder around 69.3 eV in Figure 2c in the main text originates from Br 3d electrons from the FAD membrane. The rise of the shoulder as a function of potential suggests a redistribution of the membrane's polymer branches in the catalyst layer. Depth profiling (Figure S9b) confirms that the Br is located at surface at high potentials. Such redistribution can also be observed for Nafion®-supported samples, where we probed the polymer's sulfonate groups with S2p spectra. Again, we observe an increasing peak intensity during anodization (see Figure S11), indicating that the polymer redistribution occurs on this substrate as well. However, in contrast to the case of FAD, the effect appears to be irreversible. Further support for the generality of this phenomenon comes from observations on a phosphoric acid soaked hydrocarbon membrane[7]. In this study, the driving force for the redistribution was assigned to the screening of the electrode potential, and the solvation of the ions required to do this. This interpretation can explain why there is no rise in the Br peak in Figure 2b in the main text. The dry surface for the uncovered sample does not allow for proton and anion conductivity, thus preventing the formation of an electrochemical interface. Hence, there is no interfacial potential to screen and thus no driving force for the membrane redistribution.

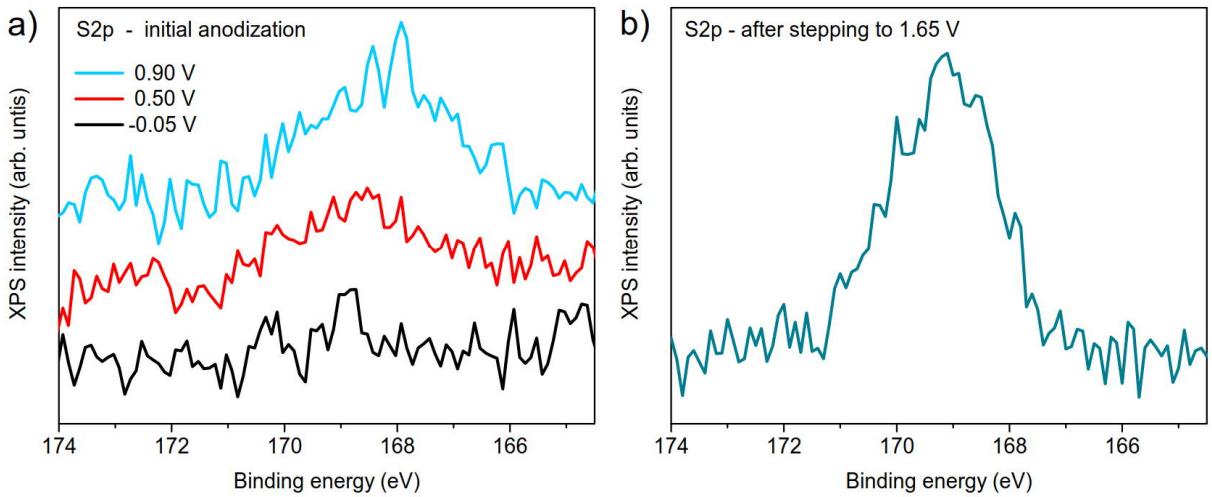

Figure S11: S2p spectra recorded during the anodization of 5 nm Pt on Nafion®. a) S2p evolution during the first anodic stepping. b) S2p spectrum after stepwise anodization up to 1.65 V_{RHE}, recorded back at 0.9V_{RHE}.

S8 Oxidation of the graphene capping layer

Despite its high chemical stability, graphene can be oxidized at sufficiently high potentials. Figure S12 shows C1s spectra recorded along with the experiment in Figure 4 in the main text. The main contributors to the spectra are graphene and the FAD substrate. The graphene is part of the working electrode, which is grounded. Hence, the C1s contribution from graphene should remain at the same position when a potential is applied. The contribution from the FAD substrate will shift however, because it is part of the electrolyte. Taking these considerations into account, only modest chemical changes are observed in the C1s spectra. At 1.85 V one can see a small peak around 288 eV, which suggests the presence of oxidized carbon. Hence, we conclude that only minor graphene oxidation occurs. We should point out however, that the C1s spectra are not a very sensitive for detecting the deterioration of graphene. Hence, there may still be some contribution of graphene oxide to the O K-edge spectra in Figure 4b in the main text. Experiments on blank graphene/FAD confirm that at potentials above 1.2 V_{RHE} some graphene oxide is observable.

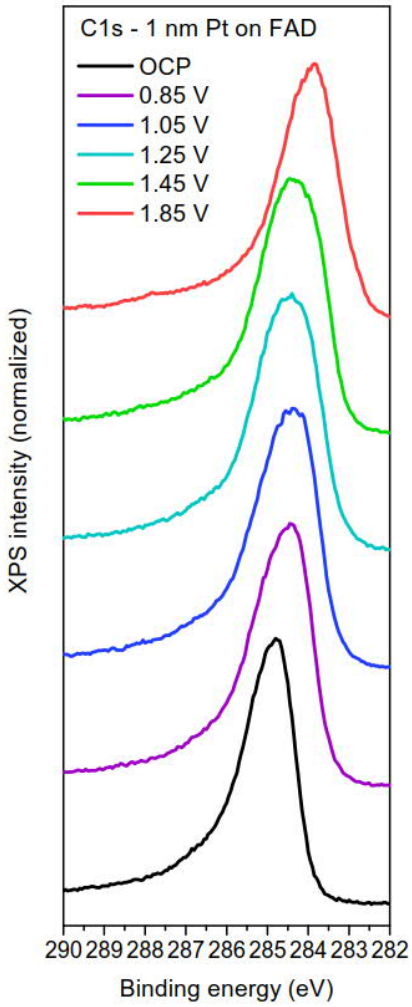

Figure S12: Evolution of C 1s spectra during the experiment depicted in Figure 4 in the main text.

S9 Bulk Pt oxidation of nanoparticles

To establish whether the oxidation of the single layer nanoparticles went all the way into the core of the particles, we recorded a Pt 4f spectrum at 1.85 V with a beam energy of 1280 eV. With an attenuation length of 1.16 nm, this measurement probes well into the bulk of the nanoparticles. Figure S13 shows that even for such a more bulk sensitive measurement, there is only a weak Pt^0 contribution, marked by a slight shoulder at 74.3 eV and a mixed Pt^0 / Br 3d peak.

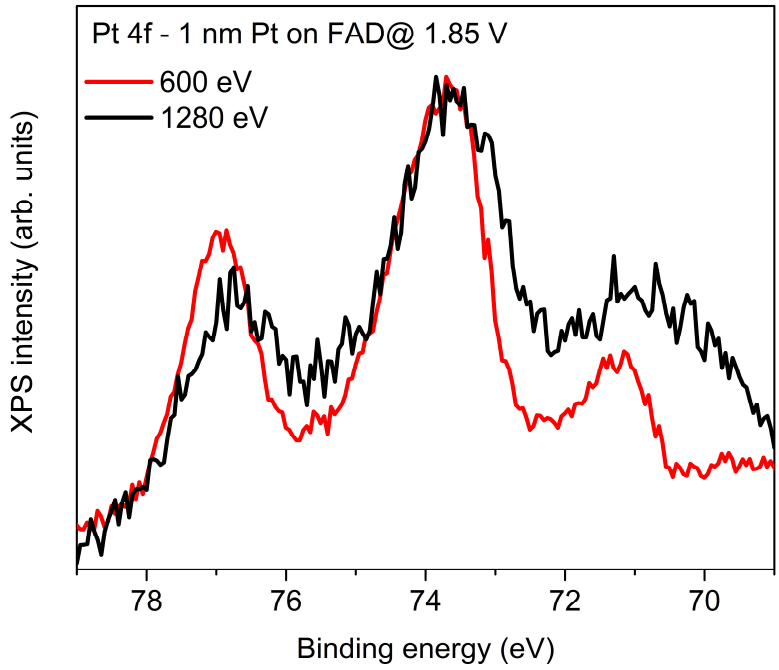

Figure S13: Pt 4f spectra of Isolated Pt nanoparticles on FAD55 in 0.1 M H_2SO_4 electrolyte at 1.85 V_{RHE}

References

(1) Saveleva, V. A.; Papaefthimiou, V.; Daletou, M. K.; Doh, W. H.; Ulhaq-Bouillet, C.; Diebold, M.; Zafeiratos, S.; Savinova, E. R. Operando Near Ambient Pressure XPS (NAP-XPS) Study of the Pt Electrochemical Oxidation in H2O and H2O/O2 Ambients. J. Phys. Chem. C 2016, 120 (29), 15930–15940.

(2) Nilsson, A.; Nordlund, D.; Waluyo, I.; Huang, N.; Ogasawara, H.; Kaya, S.; Bergmann, U.; Näslund, L.-Å.; Öström, H.; Wernet, P.; et al. X-Ray Absorption Spectroscopy and X-Ray Raman Scattering of Water and Ice; an Experimental View. J. Electron Spectros. Relat. Phenomena 2010, 177 (2–3), 99–129.

(3) Niskanen, J.; Sahle, C. J.; Juurinen, I.; Koskelo, J.; Lehtola, S.; Verbeni, R.; Müller, H.; Hakala, M.; Huotari, S. Protonation Dynamics and Hydrogen Bonding in Aqueous Sulfuric Acid. J. Phys. Chem. B 2015, 119 (35), 11732–11739.

(4) Chaturvedi, S.; Rodriguez, J. A.; Brito, J. L. Characterization of Pure and Sulfided NiMoO4 Catalysts Using Synchroton-Based X-Ray Absorption Spectroscopy (XAS) and Temperature-Programmed Reduction (TPR). Catal. Letters 1998, 51, 85–93.

(5) National Institute of Standards and Technology. NIST X-ray Photoelectron Spectroscopy Database v4.1 http://srdata.nist.gov/xps/.

(6) Cumpson, P. J.; Seah, M. P. Elastic Scattering Corrections in AES and XPS. II. Estimating Attenuation Lengths and Conditions Required for Their Valid Use in Overlayer/Substrate Experiments. Surf. Interface Anal. 1997, 25 (6), 430–446.

(7) Law, Y. T.; Zafeiratos, S.; Neophytides, S. G.; Orfanidi, A.; Costa, D.; Dintzer, T.; Arrigo, R.; Knop-Gericke, A.; Schlögl, R.; Savinova, E. R. In Situ Investigation of Dissociation and Migration Phenomena at the Pt/electrolyte Interface of an Electrochemical Cell. Chem. Sci. 2015, 6 (10), 5635–5642.